Earth Planet. Sci. Lett. 634 (2024) 118672

Contents lists available at ScienceDirect

Earth and Planetary Science Letters

journal homepage: www.elsevier.com/locate/epsl

# Metasomatism is a source of methane on Mars

Michele Rinaldi [a], Sami Mikhail [a,*], Dimitri A. Sverjensky [b]

[a] School of Earth and Environmental Sciences, University of St. Andrews, Queen's Terrace, St Andrews KY16 9TS, UK
[b] Department of Earth and Planetary Sciences, Johns Hopkins University, 3400N. Charles Street, Baltimore, MD 21218, USA

ARTICLE INFO

Edited by: Dr. F. Moynier

*Keywords:*
Methanogenesis
Mars
Fluid-rock metasomatism
Thermodynamic modelling

ABSTRACT

The abundance of inactive Martian volcanic centres suggests that early Mars was more volcanically active than today. On Earth, volcanic degassing releases climate-forcing gases such as $H_2O$, $SO_2$, and $CO_2$ into the atmosphere. On Mars, the volcanic carbon is likely to be more methane-rich than on Earth because the interior is, and was, more reducing than the present-day Terrestrial upper mantle. The reports of reduced carbon associated with high-temperature minerals in Martian igneous meteorites back up this assertion. Here, we undertake irreversible reaction path models of the fluid-rock interaction to predict carbon speciation in magmatic fluids at the Martian crust-mantle boundary. We find methane is a major carbon species between 300 and 800 °C where $\log fO_2$ is set at the Fayalite = Magnetite + Quartz redox buffer reaction (FMQ). When $\log fO_2$ is below FMQ, methane is dominant across all temperatures investigated (300–800 °C). Moreover, ultramafic rocks produce more methane than mafic lithologies. The cooling of magmatic bodies leads to the release of a fluid phase, which serves as a medium within which methane is formed at high temperatures and transported. Metasomatic methane is, therefore, a source of reduced carbonaceous gases to the early Martian atmosphere and, fundamentally, for all telluric planets, moons, and exoplanets with Mars-like low $\log fO_2$ interiors.

## 1. Introduction

Geological observations have long provided strong evidence of a subaerial hydrological system in the Martian past (Baker et al., 1991). A strong greenhouse effect early in Martian history is required to reconcile the geological reccord which requires a warmer climate. Reduced greenhouse gases (e.g., $H_2$ and $CH_4$) provide a tenable solution to explain the warming of the ancient Martian climate (Ramirez et al., 2013; Wordsworth et al., 2017; Kite et al., 2017, 2020). Indeed, a reduced Martian atmosphere is consistent with reduced chemical weathering profiles observed on Mars between 3 and 4 Ga (Liu et al., 2021; Ye and Michalski, 2022). The removal of the reduced greenhouse gases culminating in the H-poor and $CO_2$-rich present-day Martian atmosphere (Franz et al., 2017) can be explained by photochemically driven oxidation, which significantly reduces the half-life of atmospheric methane and results in the loss of $H^+$ to space (Taysum and Palmer, 2020; Zhang et al., 2021; Grenfell et al., 2022).

Martian meteorite evidence indicates that solid macro-molecular and gaseous organic carbon components (e.g., $CH_4$) are indigenous within the Martian magmas (Blamey et al., 2015). The primary source of the solid macro-molecular carbon and gaseous organic carbon components found in Martian basalts are debated (Blamey et al., 2015). However, reduced Martian carbon is associated with high-temperature magmatic minerals (e.g., olivine), suggesting a source directly from the Martian interior (Steele et al., 2012; Tsuno et al., 2018). Thus, a reduced carbon component present during Martian magmatism could be a primary source of $CH_4$ reported in the present day in the Martian atmosphere (Etiope et al., 2011; Yung et al., 2018) and possibly the source of the reduced greenhouse gases required to warm and maintain clement temperature conditions in the past (Wordsworth et al., 2017; Kite et al., 2017, 2020) (shown conceptually in Fig. 1).

On Earth, abiotic methane in geological environments is associated with carbon-bearing aqueous fluids (Peña-Alvarez et al., 2021; Zhang et al., 2023). Notably, Martian basalts are relatively reduced compared with terrestrial samples ($\log fO_2 < \Delta$FMQ -1) (Castle and Herd, 2018; Rahib et al., 2019; Nicklas et al., 2021), meaning the potential for abiotic igneous methane production is more likely on Mars than on Earth. The Martian interior is not anhydrous (Barnes et al., 2020), evidenced by the presence of hydrated magmatic minerals in Martian basalts (e.g., apatite and amphibole) (Gross et al., 2013; McCubbin et al., 2016; Davidson et al., 2020), and geochemical data show that the Martian mantle has a heterogeneous $H_2O$ distribution with estimated concentrations ranging

* Corresponding author.
*E-mail address:* sm342@st-andrews.ac.uk (S. Mikhail).

https://doi.org/10.1016/j.epsl.2024.118672
Received 25 July 2023; Received in revised form 26 January 2024; Accepted 9 March 2024
Available online 1 April 2024

from 0.01 to 2.0 wt% (Gross et al., 2013; McCubbin et al., 2016). A free-fluid phase is exsolved from silicate melts as soon as a magmatic system cools below the critical point, initially leading to a 'melt + fluid' stability field and, eventually, to the coexistence of minerals and fluids (Mysen, 2014) (pathway shown in Fig. 1). Here we quantitatively assess the potential for irreversible fluid-rock interaction driven by magmatic fluid exsolution at the Martian crust-mantle boundary as a source of atmospheric methane on Mars.

## 2. Methods

This contribution is focused on the fraction of aqueous methane generated at 0.5 GPa (isobaric) between log$fO_2$ values of ΔFMQ (Fayalite = Magnetite + Quartz redox buffer) 0 and -3, and between 300 and 800 °C. Conceptually, our models investigate the fate of carbon-rich fluids escaping from an intrusive body, eventually leading to the progressive impoverishment of carbon and fluids in the magmatic system. The fate and speciation of such fluids are determined by (i) the mineralogy and geochemistry of the rocks surrounding the intrusive body and (ii) the initial composition of the metasomatic fluids. The pressure is fixed at 0.5 GPa, which corresponds to a depth of ca. 40 km, and is consistent with data from the NASA InSight lander, which show (empirically) that the average present-day Martian crust-mantle boundary layer is between 24 and 72 km deep (Samuel et al., 2019; Knapmeyer-Endrun et al., 2021) (shown conceptually in Fig. 1). We calculate and predict carbon speciation throughout the metasomatic process and normalise the moles of each C-species to the total number of moles of carbon in the system. Therefore, the percentage of fluid hosted $CH_4$ reported in this work relates to the fraction of $CH_4$ as a function of the total amount of carbon in the fluid. During metasomatism, the fluid directly controls the precipitation of metasomatic minerals and the dissolution of the host rock. A step-by-step evolution of the metasomatic system is calculated, where each unit of the reaction progress corresponds to 1.0 mol of the reactant rock being destroyed and absorbed by the fluid. The fluid-rock interaction proceeds until thermodynamic equilibrium is achieved. The modelling results in the fluid speciation of aqueous anions, metal complexes, and neutral species, alongside the mineralogical and geochemical evolution of metasomatic minerals. During metasomatism, the reactant rock is progressively consumed by the fluid, modifying the geochemistry of the fluid and co-genetic metasomatic minerals.

### 2.1. Deep Earth Water model

The Deep Earth Water model (DEW) is thermodynamic software which allows the theoretical geochemical calculation of fluid-rock interaction using the Helgeson – Kirkham – Flowers (HKF) equations of state for aqueous species (Helgeson and Kirkham, 1974a, 1974b, 1976; Helgeson et al., 1981; Shock et al., 1997; Shock and Helgeson, 1988; Sverjensky et al., 2014a; Huang and Sverjensky, 2019; Sverjensky, 2019) up to 6 GPa and 1200 °C. The equilibrium constants for aqueous complexes are calculated through the DEW model, and equilibrium constants for minerals are taken from Berman (1988) or by fitting the Berman (1988) equations to experimental data. The equilibrium constants for solid and dissolved species are incorporated in the aqueous speciation, solubility, and chemical mass transfer codes EQ3 and EQ6 (Wolery, 1992). The latter codes have been adapted for elevated pressures and temperatures. They are widely used to model aqueous speciation and irreversible chemical mass transfer during fluid-rock interactions from weathering conditions to deep Earth conditions (Mikhail and Sverjensky, 2014; Sverjensky et al., 2014b; Sverjensky and Huang, 2015; Mikhail et al., 2017, 2021; Rinaldi et al., 2023; Huang and Sverjensky, 2020). In the first step, the composition and speciation of the fluid in equilibrium with the initial lithology are calculated with the aqueous speciation and solubility code EQ3. Then, the fluid interacts with a different rock under isobaric and isothermal conditions. Because the fluid-rock system is not in equilibrium, a chemical gradient drives irreversible mass transfer reactions, which are run using the mass transfer code EQ6 calibrated for upper mantle conditions (Huang and Sverjensky, 2019; Sverjensky, 2019). More details about the complexity of the theoretical approach to thermodynamic modelling can be found in previous literature (Miron et al., 2019; Sverjensky, 2019) and the examples cited above. The DEW model considers every mineral as intrinsically connected to a specific reaction (Sverjensky, 2019), such as the example shown below:

$$Forsterite + 2\ H^+ \rightarrow Mg^{2+} + 0.5\ H_4SiO_4(aq) \quad (1)$$

Eq. (1) shows the dissolution reaction, which defines the relationship between a mineral (forsterite) and its fluid species ($H^+$, $Mg^{2+}$, and $H_4SiO_4$). The same concept is applied to all other mineral components. Thermodynamics allows the calculation of the Gibbs Free energy for a reaction, shown in Eq. (2):

$$\Delta G_{r_{P,T}} = \Delta G^0_{r_{P,T}} + 2.303RTlogQ \quad (2)$$

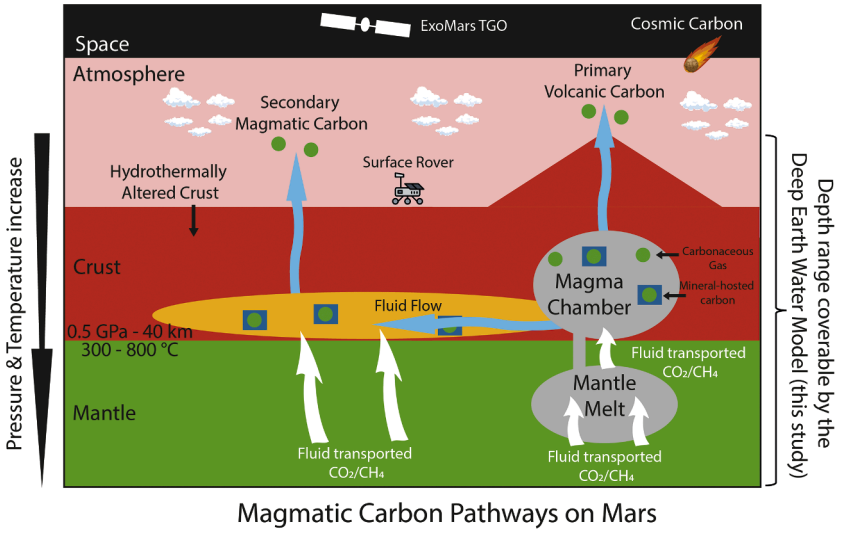


Magmatic Carbon Pathways on Mars

**Fig. 1.** Cartoon illustrating sources of carbon on Mars which showcases the focus of our research and our modelling approach. No spatial dimensions are considered in our model, *sensu stricto*. Instead, we control pressure, temperature, and composition and set these to correspond to the desired depth of a Martian subsurface environment.

where $\Delta G_{rP,T}$ is the Gibbs free energy of reaction at a specific temperature $T$ (K) as a function of the Standard Gibbs Free energy of reaction ($\Delta G^0_{r\,P,T}$), the gas constant ($R = 8.314$ J K$^{-1}$ mol$^{-1}$), and the thermodynamic activity quotient ($Q$). At equilibrium conditions, $\Delta G^0_{r\,P,T} = 0$. In this specific case, Eq. (2) can be re-written as:

$$logK = \frac{\Delta G^0_{r\,P,T}}{-2.303RT} \tag{3}$$

and

$$K = \Pi_i (a_i)^{\nu_i} \tag{4}$$

$K$ is the thermodynamic equilibrium constant, which defines a fixed activity ratio for the species in the reaction at a given pressure and temperature. It should be noted that the ratio is fixed, but the value of each species' chemical activity ($a_i$) involved varies, with $\nu_i$ being the stoichiometric reaction coefficient for the i$^{th}$ species in a reaction. When $K > 1$, there are more products than reactants; when $K < 1$, there are more reactants than products. The equilibrium constant $K$ is sensitive to pressure and temperature, and the system equilibrium varies as a function of the environmental conditions (pressure, temperature, $fO_2$, pH and bulk composition).

#### 2.1.1. Evaluation of equilibrium constants over a wide range of pressure and temperatures

The evaluation of the equilibrium constant is a key feature in computing aqueous speciation, solubility, and mass transfer models. Traditionally, in aqueous geochemistry, the computer code SUPCRT92 has been used to calculate the $K$ value of dissociation reactions, but it is limited to 1000 °C and 0.5 GPa. In contrast, the DEW model can calculate the equilibrium constants up to 1200 °C and 6.0 GPa, as the dielectric constant of water has been extended by Sverjensky et al. (2014a) up to these pressure-temperature conditions. The definition of $\Delta G^0_{r\,P,T}$ at high temperature and pressure is required to calculate log$K$. To do this, we need the standard Gibbs free energy for each species involved in a reaction, shown in Eq. (5):

$$\Delta G^0_{r\,P,T} = \Sigma_j\ \nu_j\ \Delta G^0_{f\,j\,P,T} \tag{5}$$

where:

$$\Delta G^0_{r\,P,T} = \Delta G^0_{f\,j\,Pr,Tr} + \left(\Delta G^0_{j\,P,T} - \Delta G^0_{j\,Pr,Tr}\right) \tag{6}$$

The first term on the right-hand side of Eq. (6) refers to the true standard Gibbs free energy of formation of j$^{th}$ at reference pressure and temperature. In contrast, the second term refers to the variation of the Gibbs free energy of the j$^{th}$ species with temperature and pressure. If the first term is available in the literature for many minerals and aqueous species, the lack of experimental data for high pressure and temperature conditions requires theoretical estimation.

If we define:

$$G^0_{j\,P,T} - G^0_{j\,Pr,Tr} = -S^0_{j\,Pr,Tr}(T - T_r) + \int_{Tr}^{T} C^0_{j\,Pr} dT - T\int_{Tr}^{T} C^0_{j\,Pr} dlnT + \int_{Pr}^{P} V^0_{j\,T} dP \tag{7}$$

It is evident that the standard partial molal entropy at the reference temperature and pressure ($S^0_{j\,Pr,Tr}$ [J mol$^{-1}$ K$^{-1}$]), the temperature dependence of the isobaric standard partial molal heat capacity ($C^0_j Pr$ [J mol$^{-1}$ K$^{-1}$]), and the pressure dependence of the standard partial molal volume ($V^0_{j\,T}$ [cm$^3$ mol$^{-1}$]) are required to calculate the change in the Gibbs free energy of a species with pressure and temperature.

#### 2.1.2. Mineral free energies at high pressures and temperatures: Berman equations

The thermoelastic properties of minerals are calculated through the approach proposed by Berman (1988) using the following equations:

$$C^0_{j\,Pr} = k_1 + k_2 T^{-0.5} + kT^{-2} + k_4 T^{-3} \tag{8}$$

$$\frac{V_{P,T}}{V_{Pr,Tr}} = 1 + v_1(P - P_r) + v_2 + (P - P_r)^2 + v_3(T - T_r) + v_4(T - T_r)^2 \tag{9}$$

Where k$_1$, k$_2$, k$_3$, k$_4$, v$_1$, v$_2$, v$_3$ and v$_4$ are empirical parameters fit to experimental data. The partial molal entropy ($S^0_{j\,Pr,Tr}$) and partial molal enthalpy ($\Delta G^0_{j\,Pr,Tr}$) are available for numerous minerals in Berman (1988). $V_{Pr,Tr}$ is obtained by experimental values.

#### 2.1.3. Aqueous species free energies at high pressures and temperatures: Helgeson – Kirkham – Flowers (HFK) equations of state

Equations of state for modelling aqueous species modelling at elevated temperatures and pressures are crucial. Many different approaches have been proposed and discussed in the literature (Anderson, 2017; Miron et al., 2019). No equation best suits every pressure-temperature condition, especially at extreme conditions such as close to the supercritical point of water. The DEW model is based on the Helgeson – Kirkham – Flowers (HKF) approach (Helgeson and Kirkham, 1974a, 1974b, 1976; Helgeson et al., 1981), which forms the base for all the subsequent revisions and extensions (Shock et al., 1997; Shock and Helgeson, 1988; Sverjensky et al., 1997, 2014a; Huang and Sverjensky, 2019; Sverjensky, 2019). For ease of readability, here we present summary versions of the HFK equations of state, listed as Eqs. (10)–(13):

$$H^0_j = H^R_j + f_{Hi}\ (a_1,\ \ldots,\ a_4,\ c_1,\ c_2,\ \omega) \tag{10}$$

$$G^0_j = G^R_j - S^R_j(T - T^R) + f_{Gi}\ (a_1,\ \ldots,\ a_4,\ c_1,\ c_2,\ \omega) \tag{11}$$

$$S^0_j = S^R_j + f_{Si}\ (a_1,\ \ldots,\ a_4,\ c_1,\ c_2,\ \omega) \tag{12}$$

$$C^0_j = C^R_j + f_{Ci}\ (a_1,\ \ldots,\ a_4,\ c_1,\ c_2,\ \omega) \tag{13}$$

Where the parameters between brackets are the equation of state coefficients for the individual aqueous species. The superscript R refers to the reference temperature and pressure. As the Born solvation coefficient ω is involved in the HKF method for calculating solvation effects using the dielectric constant of water, a characterisation of pure water is needed. The dielectric constant of water has been calibrated up to 6 GPa and 1200 °C (Sverjensky et al., 2014a). The primary use of Eqs. (10)–(13) allows calculation and prediction of each aqueous species' standard partial molal free energies, from simple and monoatomic ions to neutral species, complexes, and organic compounds. The integrated free energies are less sensitive to uncertainty than the derivative properties such as heat capacity and volume, as the HKF approach was built on the need for estimation algorithms in the perspective of the lack of derivative properties for most aqueous species at high pressure and temperatures. Ideally, these equations would be fitted to experimental data over a broad range of conditions. Sadly, the current scientific literature does not provide experimental data at "geological" pressures and temperatures. The built-in estimation algorithm has, therefore, proved to be an unmatched strength of the HKF approach. However, a common situation is that no experimental volumes, compressibilities, and heat capacities are available even at 25 °C and 1.0 bar. This is most common for aqueous metal complexes, both inorganic and organic. The DEW model has implemented an estimation algorithm (Shock et al., 1997; Sverjensky et al., 1997) to compensate for this lack of empirical data. Consequently, a completely predictive scheme is available.

### 2.2. The modelling approach

Once the chemical and thermoelastic parameters for each phase in the system have been defined, the thermodynamic modelling of an aqueous system is possible. A mathematical system is considered where all the reactions involving aqueous species are calculated simultaneously:

$$logK_j = \frac{\Delta G^0_{r,\,jP,T}}{-2.303RT} \quad (14)$$

$$m_{k,\,fluid} = \Sigma m_{k,j} \quad (15)$$

$$q_{k,\,fluid} = \Sigma q_{k,j} \quad (16)$$

Eq. (14) is Eq. (3) applied for all the aqueous species in the fluid. Eqs. (15) and (16) are mass and charge balances between the fluid and the aqueous species. Solving this system will result in a unique solution (the number of equations is equal to the number of variables) for the activity and concentration of each aqueous phase and, therefore, the composition and speciation of the fluid. Finally, the fluid's saturation state concerning the minerals can be calculated by applying Eq. (2) for each possible mineral dissolution reactions. Because the fluid changes composition at each step of the metasomatic reaction (where each unit of the reaction progress corresponds to 1.0 mol of the reactant rock being destroyed), this mathematical system is solved for each step with a new set of results. As each mineral phase is intrinsically related to the fluid speciation, the resulting geochemistry of the fluid phase leads to the precipitation of new metasomatic minerals. Therefore, it is possible to simulate the fluid-rock interaction as the magnitude of the metasomatic interaction progressively increases and evaluate the influence of the host rock over the fluid, and *vice-versa*.

### 2.3. Composition of Martian systems

The dominant lithology in the Martian mantle is peridotite, but the precise composition and mineralogy are not well constrained. Therefore, we arbitrarily chose that the model fluids are initially in equilibrium with a spinel peridotite (peridotitic fluid) (Howarth et al., 2014) to investigate if the country rock plays a critical role in methanogenesis during fluid-rock interaction at relevant P-T conditions (0.5 GPa, 300–800 °C) (Samuel et al., 2019; Knapmeyer-Endrun et al., 2021) (Table 1). We used redox conditions compatible with the Martian crust and mantle ($\log fO_2$ = ΔFMQ -3 to 0), determined by electron microprobe analysis of Fe-Ti oxides on Martian basalts (Castle and Herd, 2018; Rahib et al., 2019; Nicklas et al., 2021). Despite the redox conditions suggesting graphite is stable under the environmental conditions used in this work (Hirschmann and Withers, 2008), we did not model aqueous carbon in equilibrium with graphite due to uncertainties in the activity coefficient of aqueous $CO_2$. Instead, for most models, we set the amount of carbon at 0.5 molal. At 600 °C and $\log fO_2$ = ΔFMQ -2, we also varied the amount of carbon from 0.1 to 2.0 molal to study its influence on carbon speciation. Then, the fluids are forced to interact with a broad range of lithologies. The lithological composition of Martian interiors is largely unknown, aside from assuming a peridotitic mantle and mafic crust, and the only available data about igneous rocks are from meteorites. To avoid introducing further uncertainties, a range of compositions spanning the mafic and ultramafic rocks found as Martian meteorites were considered in this work. We selected a series of samples with an estimated equilibration pressure of 0.5 GPa, and we used their geochemistry to constrain the mineralogy and geochemistry of reactant rocks as follows: lherzolite (Howarth et al., 2014), dunite (Beck et al., 2006), clinopyroxenite (Treiman, 2005), orthopyroxenite (Gleason et al., 1997), and gabbro (Udry et al., 2017) (Table 2). We also simulated a range of initial fluid/rock ratios (from 0.1 to 10), defined as the number of moles of water over the number of moles of reactant rock, to consider different metasomatic conditions. The fluid/rock ratio slightly changes during the modelling phase as water is an active phase in the system and can be formed or consumed during the chemical reactions, as well as the reactant minerals.

## 3. Results

We find that fluid metasomatism of peridotite, eclogite, and gabbro on Mars results in the precipitation of various metasomatic minerals comprising oxides, hydroxides, silicates, carbonates, and native carbon (Table S1). For systems where carbon molality is $< 2.0$, we find no relationship between the carbon content of the system and carbon speciation (Fig. 2a). The most abundant carbon species in our fluids are $CH_4$, $CO_2$ and $H_2CO_3$, followed by $NaHCO_3$ and $HCO_3^-$ (Fig. 2c and d, Table S2). Solid carbonaceous phases such as graphite and (Ca-, Mg-) carbonate are rare, precipitating only when the fluid reacts with a gabbro at 300 °C across a range of $\log fO_2$ in this study. For temperatures $> 400$ °C, graphite and (Ca-, Mg-) carbonate are dissolved into the fluid (Table S1). The full dataset of [1] initial and final carbon speciation, [2]

**Table 2**
Mineralogical and solid solution compositions of mantle rocks used during fluid-rock interaction (ol: olivine; opx: orthopyroxene; cpx: clinopyroxene; pl: plagioclase; mag: magnetite). Magnetite is considered a pure phase.

| Rock | Mineral composition (% in volume) |
|---|---|
| Lherzolite | 55 % ol ($Fo_{0.65}$), 35 % opx ($En_{0.75}Fs_{0.25}$), 10 % cpx ($Di_{0.26}Hd_{0.22}Ja_{0.01}En_{0.51}$) |
| Dunite | 90 % ol ($Fo_{0.78}$), 1 % opx ($En_{0.80}Fs_{0.20}$), 4 % cpx ($Di_{0.40}Hd_{0.12}Ja_{0.01}En_{0.47}$), 5 % mag |
| Clinopyroxenite | 15 % ol ($Fo_{0.45}$), 80 % cpx ($Di_{0.26}Hd_{0.30}Ja_{0.01}En_{0.43}$), 3 % pl ($Ab_{0.59}An_{0.37}Kf_{0.04}$), 2 % mag |
| Orthopyroxenite | 95 % opx ($En_{0.70}Fs_{0.30}$), 5 % mag |
| Gabbro | 2 % ol ($Fo_{0.05}$), 46 % cpx ($Di_{0.12}Hd_{0.43}Ja_{0.01}En_{0.44}$), 50 % pl ($Ab_{0.48}An_{0.52}Kf_{0.00}$), 2 % mag |

**Table 1**
Chemical composition (molality: moles/kg) for selected peridotitic fluids at $fO_2$ = ΔFMQ 0 and 0.5 GPa, between 300 and 800 °C. All the fluid compositions for different temperatures, $fO_2$ and carbon content are available in the Supplementary Material.

| Molality (mol/kg) | Equilibrium with | 300 °C | 400 °C | 500 °C | 600 °C | 700 °C | 800 °C |
|---|---|---|---|---|---|---|---|
| Na | Fixed | 0.50 | 0.50 | 0.50 | 0.50 | 0.50 | 0.50 |
| K | Fixed | 0.50 | 0.50 | 0.50 | 0.50 | 0.50 | 0.50 |
| Ca | Diopside (0.26) | $0.22 \times 10^{-5}$ | $0.85 \times 10^{-5}$ | $0.22 \times 10^{-4}$ | $0.59 \times 10^{-4}$ | $0.15 \times 10^{-4}$ | $0.30 \times 10^{-3}$ |
| Mg | Forsterite (0.65) | 0.17 | 0.28 | 0.32 | 0.30 | 0.25 | 0.19 |
| Fe | Fayalite (0.35) | $0.34 \times 10^{-4}$ | $0.18 \times 10^{-3}$ | $0.38 \times 10^{-3}$ | $0.37 \times 10^{-3}$ | $0.41 \times 10^{-3}$ | $0.47 \times 10^{-3}$ |
| Si | Enstatite (0.41) | 0.06 | 0.01 | 0.16 | 0.24 | 0.28 | 0.30 |
| Al | Spinel | 0.14 | 0.15 | 0.21 | 0.26 | 0.27 | 0.26 |
| C | Fixed | 0.50 | 0.50 | 0.50 | 0.50 | 0.50 | 0.50 |
| Cl | Fixed | 0.50 | 0.50 | 0.50 | 0.50 | 0.50 | 0.50 |
| pH | Charge balance | 8.08 | 7.58 | 7.38 | 7.30 | 7.27 | 7.32 |
| $\log fO_2$ | | -35.45 | -28.72 | -23.81 | -20.07 | -17.13 | -14.75 |
| ΔFMQ | | 0 | 0 | 0 | 0 | 0 | 0 |

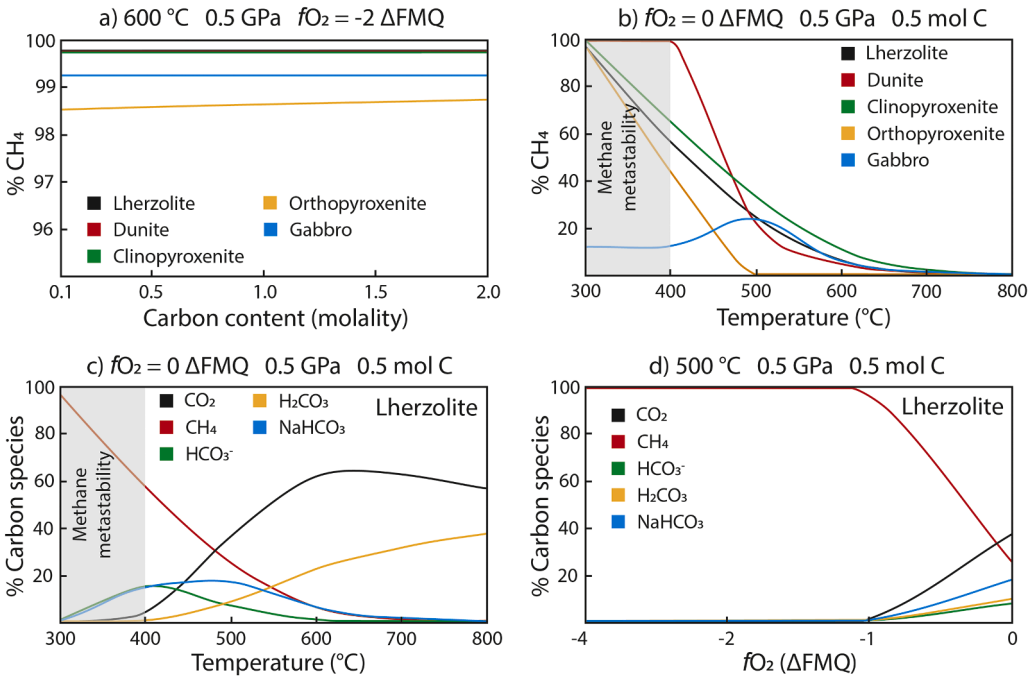


**Fig. 2.** Fraction of methane during the evolution of fluid-rock metasomatism. The main findings of this work plotted to show the fraction of methane in the fluid during metasomatism of a range of Martian lithologies as a function of carbon content (a) and temperature (b), and the relative proportion of carbon species as a function of temperature (c) and oxygen fugacity (d). We find that the fraction of methane increases as the temperature and oxygen fugacity decrease. The total amount of carbon in the system does not affect carbon speciation. Methane metastability is reported as a grey field (Manning et al., 2013). Fluid/rock ratio = 1.85 [mol/mol].

fluid compositions, [3] the mineralogical composition of resulting rocks, and [4] the variation in redox conditions are provided as an external Excel file accessible at this link: 10.17630/47001927-ab36-40d6-9429-58001a1fc69c.

### 3.1. *Methanogenesis as a function of host rock lithology*

Abiotic methanogenesis is efficient when the fluid is equilibrated with ultramafic rocks, especially peridotites (Fig. 2b). Conversely, fluid-

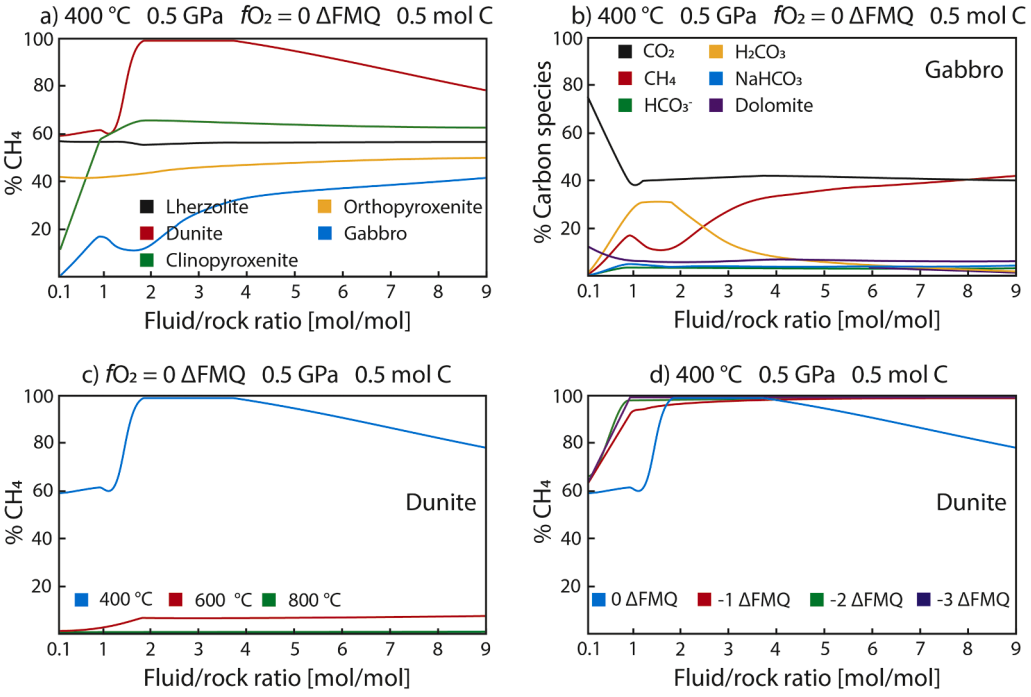


**Fig. 3.** Influence of fluid/rock ratio on carbon speciation. The fluid/rock ratio has a significant influence on the speciation of carbon during metasomatic reactions when fluids interact with dunite, clinopyroxenite, and gabbro, but shows no significant influence when fluids interact with lherzolite and orthopyroxenite at 400 °C (a-b). However, the fluid/rock ratio shows no significant influence on the speciation of carbon during metasomatic reactions when fluids interact with dunite at $T \geq$ 400 °C (c), and the influence of the fluid/rock ratio varies as a function of $fO_2$ (d).

rock interaction with more felsic rocks, such as gabbro, results in more oxidising conditions with the subsequent precipitation of graphitic and carbonate mineral phases, thus subtracting carbon from the fluid and reducing the mass of methane. Variations in the amount of methane between 300 and 600 °C between lithologies reflect the stability of each mineral assemblage when reacting with the fluid at the selected P-T-X, which forces oscillations in the redox conditions of the system. Negative changes in oxygen fugacity ($\Delta \log fO_2$) are observed when fluids react with lherzolite, dunite and clinopyroxenite. Conversely, for models involving orthopyroxenite and gabbro, the $\Delta \log fO_2$ is positive and significant for the stability of methane. An increase in the oxygen fugacity results in the destabilisation of $CH_4$ in favour of more oxidised species such as $CO_2$, $H_2CO_3$, and solid phases such as graphite and dolomite (Table S1).

### 3.2. Methanogenesis as a function of fluid/rock ratio

In our models, methanogenesis is influenced by the fluid/rock ratio when the fluid interacts with dunite, gabbro, and clinopyroxenite at low temperatures (400 °C). Still, for systems involving lherzolite and orthopyroxenite or for temperatures > 400 °C (with the exception of dunite), the fluid/rock ratio is effectively insignificant (Fig. 3). In the first case, the concentration of methane produced during a metasomatic process varies in a non-linear progression alongside the fluid/rock ratio at low temperatures (400 °C) (Fig. 3) and at relatively oxidised conditions ($\log fO_2 = \Delta$FMQ 0) (Fig. 3). Therefore, progressive increment of the fluid content in the system related to the exsolution of water from the cooling of a magmatic body strongly influences methanogenesis for systems with fluid/rock ratios < 2 [mol/mol]. Conversely, where the fluid/rock ratio > 2, the amount of methane produced by metasomatic interactions can be considered constant unless the reactant lithology is dunite (although $CH_4$ still comprises > 60 % of the carbon species under these conditions; Fig. 3).

## 4. Discussion

### 4.1. Metasomatic methanogenesis around cooling plutons on Mars

The thermal evolution of mantle potential temperatures within telluric planets follows a rule whereby the temperature was higher in the deep past (30–40 K $Gyr^{-1}$; Stevenson, 2003; Baratoux et al., 2011), and this means Mars may have also experienced the emplacement of ultramafic intrusions (high-Mg rocks) because adiabatic gradients would have been hotter (akin to Earth and the Moon). If so, this would provide an environment for methane production during fluid-rock metasomatism (being Mg-rich; see trends in Fig. 2b).

The increase in methane abundance with decreasing temperature shown here (Fig. 2b-c) is coherent with theoretical and experimental data from the literature constrained to an equilibrium between carbonates, graphite, and diamond with carbon-rich aqueous species (Zhang and Duan, 2009; Dalou et al., 2019). These data also speak to observations of fluid-rock interaction as a source of abiotic methane in nature (Boutier et al., 2021; Piercy et al., 2022; Wang et al., 2022). Moving forward, our dataset exposes and highlights the role played by silicates in controlling carbon speciation because we show that mafic and ultramafic lithologies have different influences on abiotic methanogenesis (Fig. 2b).

The cooling of these fluid systems, associated with the lower oxygen fugacity of the Martian mantle and crust (Nicklas et al., 2021), promotes suitable conditions for abiotic methanogenesis in a magmatic environment, developing progressive $CH_4$-richer fluids as the temperature drops (Fig. 2c). The influence of temperature and lithology over carbon speciation is mitigated by lowering the oxygen fugacity (Figs. 2d, S3). We predict a reduction in the concentration of $NaHCO_3$ and $HCO_3^-$ where $\log fO_2 = \Delta$FMQ -1, and, instead, carbon is stabilised mainly in $CH_4$, $H_2CO_3$ and $CO_2$ (Fig. 2c-d). Where $\log fO_2 \leq \Delta$FMQ -2 (common for the Martian interior; Rahib et al., 2019; Nicklas et al., 2021), methane is always the dominant carbon species. Therefore, our models show that the production and preservation of abiotic methane are feasible over a broad range of conditions, and methane production and preservation are strongly affected by the mineralogy of the reactant rock, especially for oxidised systems (e.g., where $\log fO_2 = \Delta$FMQ > 0).

### 4.2. Metasomatic methanogenesis in the Martian crust

Although our models predict methane preservation below 400 °C, it is well-established that methanogenic reactions are very slow below this threshold (Shock, 1988; Manning et al., 2013). It is thus possible that aliphatic and condensed polycyclic aromatic hydrocarbons are expected instead of gaseous $CH_4$ (Zolotov and Shock, 1999, 2000), akin to what is observed in the meteorite record (Webster et al., 2013 Steele et al., 2012). Thermodynamically speaking, methane would be a metastable species at $T < 400$ °C (Fig. 2), meaning that it is not in equilibrium with the other carbon species. $CH_4$ should not react with the fluid or rocks when stored and possibly when transported along steep adiabats toward the surface due to its kinetic reluctance to participate in reactions (Shock, 1988; Sverjensky et al., 2020). Therefore, fluid traps located at the Martian mantle-crust boundary can store the $CH_4$ during the progressive cooling of a metasomatic system and preserve it over geological time, providing a shallow crustal source for atmospheric methane.

Metasomatic fluid generated in the Martian crust can reach the surface through deep fractures, typical of the brittle Martian crust (Heap et al., 2017), resulting in effusive degassing after magma emplacement on Mars (Wetzel et al., 2013). Therefore, it is possible that metasomatic methane production contributed to the release of $CH_4$ into the Martian atmosphere, past and present. A greater magmatic flux on early Mars – consistent with surface observations and thermal models – would have translated to a greater methane flux and thus contributed to the greenhouse effect (Montesi and Zuber, 2003; Ramirez et al., 2013) required to explain geological evidence for an active hydrological cycle on the surface. The loss of the Martian geodynamo could have catalysed the photochemical disassociation of water and methane (Taysum and Palmer, 2020; Zhang et al., 2021; Grenfell et al., 2022) over time, resulting in a $CO_2$-dominated atmosphere as observed presently. Ergo, abiotic methane production in the crust cannot be ruled out as a source of methane in both past and present-day Martian atmosphere.

Using the percentage of methane over the total carbon obtained in our models, it is possible to run a preliminary calculation of the amount of methane formed in a given system. We utilise:

$$m_{CH_4} = V_{rock} \cdot \rho_{rock} \cdot \frac{1}{M_{rock}} \cdot X_{fluid} \cdot M_{water} \cdot b_{carbon} \cdot X_{CH_4} \cdot M_{CH_4} \quad (17)$$

Where $m_{CH_4}$ = mass of methane in the fluid [g], $V_{rock}$ = volume of the reactant rock [$m^3$], $\rho_{rock}$ = density of the reactant rock [$kg/m^3$], $M_{rock}$ = molar mass of the reactant rock [g/mol], $X_{fluid}$ = fluid/rock ratio [mol/mol], $M_{water}$ = molar mass of water [g/mol], $b_{carbon}$ = carbon molality [mol/kg], $X_{CH_4}$ = fraction of methane over the total carbon of the system, and $M_{CH_4}$ = molar mass of methane [g/mol].

Considering a fluid bearing 600 ppm of carbon (0.5 molal) in a system with a fluid/rock ratio [mol/mol] of 1.85, at 0.5 GPa, 400 °C and $\log fO_2 = \Delta$FMQ 0, up to 9850 of methane can be produced per 1 $m^3$ of rock during fluid-rock metasomatism (see Table 3). As different lithologies have different densities, we report the calculated density [$kg/m^3$], molecular weight [g/mol], and fluid/rock ratio [mol/mol] for each lithology (Table 3). These parameters are calculated from mineral compositions presented in Table 2. As Martian rocks are Fe-enriched relative to their Terrestrial counterparts, the average density of each Martian lithology is higher than the same rock would be with an Earth-like mantle Fe/Mg ratio.

**Table 3**
Amount of methane (grams) for $m^3$ of rock involved in fluid-rock interaction at 400 °C, 0.5 GPa and $fO_2$ = ΔFMQ 0.

| Lithology | Rock density ($kg/m^3$) | Rock molecular weight (g/mol) | Fluid/rock ratio (mol/mol) | $CH_4$ / $C_{total}$ | $CH_4$ (g) / $m^3$ of reactant rock |
|---|---|---|---|---|---|
| Lherzolite | 3102 | 96.4 | 1.85 | 0.57 | 4903 |
| Dunite | 3125 | 84.8 | 1.85 | 1.00 | 9850 |
| Clinopyroxenite | 3295 | 160.4 | 1.85 | 0.65 | 3569 |
| Orthopyroxenite | 3532 | 114.3 | 1.85 | 0.44 | 3634 |
| Gabbro | 3079 | 208.9 | 1.85 | 0.12 | 473 |

## 5. Conclusions

Irreversible reaction path models of the fluid-rock interaction predict that methane is a major carbon species between 300 and 800 °C where log$fO_2$ is set at the Fayalite = Magnetite + Quartz redox buffer reaction in the Martian crust. When log$fO_2$ is below FMQ, methane dominates all temperatures investigated (300–800 °C). We find that the geochemistry of the reactant rocks plays a crucial role in carbon speciation during fluid-metasomatism. Lherzolite and clinopyroxenite produce similar proportions of carbon species to one another, whereas dunite is the most suitable rock for methane production. Between 300 and 600 °C, orthopyroxenite and gabbro produce less $CH_4$ than other lithologies due to oxygen fugacity variations triggered during the metasomatic reactions. Fluid-rock interaction involving ultramafic rocks produces more methane than when mafic lithologies are considered, highlighting the role of lithology during methanogenesis. However, for $T \geq 700$ °C, all models predict a similar proportion of methane production regardless of the reactant mineralogy and oxygen fugacity.

Fluids exsolved from magmatic bodies are important vessels for producing and transporting methane from the Martian interiors to the atmosphere. Metasomatic methane is, therefore, a source of reduced carbonaceous gases to the early Martian atmosphere and, potentially, for igneous systems on all telluric planets, and moons. Furthermore, these results are directly transferable to exoplanet science. For example, future chemical characterisation of exoplanet atmospheres via space-borne telescopes should strongly question the notion that disequilibrium carbon in the atmospheres of volcanically active telluric bodies (i.e., the coexistence of $CO_2 + CH_4$) might serve as a reliable biosignature.

## CRediT authorship contribution statement

**Michele Rinaldi:** Writing – review & editing, Writing – original draft, Visualization, Methodology, Formal analysis, Data curation. **Sami Mikhail:** Writing – review & editing, Writing – original draft, Visualization, Supervision, Project administration, Methodology, Investigation, Funding acquisition, Formal analysis, Data curation, Conceptualization. **Dimitri A. Sverjensky:** Writing – review & editing, Writing – original draft, Supervision, Software, Methodology, Investigation, Formal analysis.

## Declaration of competing interest

The authors declare no competing interests.

## Data availability

The data that support the findings of this study are available in the St Andrews' Research Information System (PURE) with the identifier 10.17630/47001927-ab36-40d6-9429-58001a1fc69c.

## Acknowledgments

MR and SM acknowledge support from NERC standard grant (NE/PO12167/1) and UK Space Agency Aurora grant (ST/T001763/1). DAS acknowledges support by the U.S. Department of Energy, Office of Science, Basic Energy Sciences, Geosciences program under Award Number DE-SC0019830 as well as NSF Petrology and Geochemistry Grant Number 2032039. We are grateful to Fabrice Gaillard and Claire Marie Guimond for their constructive reviews, which greatly improved the clarity of the manuscript, and for the supportive editorial handling of Frédéric Moynier.

## Supplementary materials

Supplementary material associated with this article can be found, in the online version, at doi:10.1016/j.epsl.2024.118672.

## References

Anderson, G., 2017. Thermodynamics of natural systems, second edition. Cambridge University Press. https://doi.org/10.1017/9781316796856.
Baker, V.R., Strom, R.G., Gulick, V.C., Kargel, J.S., Komatsu, G., Kale, V.S., 1991. Ancient oceans, ice sheets and the hydrological cycle on Mars. Nature 352, 589–594. https://doi.org/10.1038/352589a0.
Baratoux, D., Toplis, M.J., Monnereau, M., Gasnault, O., 2011. Thermal history of Mars inferred from orbital geochemistry of volcanic provinces. Nature 472, 338–341. https://doi.org/10.1038/nature09903.
Barnes, J.J., McCubbin, F.M., Santos, A.R., Day, J.M.D., Boyce, J.W., Schwenzer, S.P., Ott, U., Franchi, I.A., Messenger, S., Anand, M., Agee, C.B., 2020. Multiple early-formed water reservoirs in the interior of Mars. Nat. Geosci. 13, 260–264. https://doi.org/10.1038/s41561-020-0552-y.
Beck, P., Barrat, J.A., Gillet, P., Wadhwa, M., Franchi, I.A., Greenwood, R.C., Bohn, M., Cotten, J., van de Moortèle, B., Reynard, B., 2006. Petrography and geochemistry of the chassignite Northwest Africa 2737 (NWA 2737). Geochim. Cosmochim. Acta 70, 2127–2139. https://doi.org/10.1016/J.GCA.2006.01.016.
Berman, R.G., 1988. Internally-consistent thermodynamic data for minerals in the system $Na_2O$-$K_2O$-CaO-MgO-FeO-$Fe_2O_3$-$Al_2O_3$-$SiO_2$-$TiO_2$-$H_2O$-$CO_2$. J. Petrol. 29, 445–522. https://doi.org/10.1093/PETROLOGY/29.2.445.
Blamey, N.J.F., Parnell, J., McMahon, S., Mark, D.F., Tomkinson, T., Lee, M., Shivak, J., Izawa, M.R.M., Banerjee, N.R., Flemming, R.L., 2015. Evidence for methane in Martian meteorites. Nat. Commun. 6, 1–7. https://doi.org/10.1038/ncomms8399.
Boutier, A., Vitale Brovarone, A., Martinez, I., Sissmann, O., Mana, S., 2021. High-pressure serpentinization and abiotic methane formation in metaperidotite from the Appalachian subduction, northern Vermont. Lithos 396–397, 106190. https://doi.org/10.1016/J.LITHOS.2021.106190.
Castle, N., Herd, C.D.K., 2018. Experimental investigation into the effects of oxidation during petrogenesis of the Tissint meteorite. Meteorit. Planet. Sci. 53, 1341–1363. https://doi.org/10.1111/MAPS.13083.
Dalou, C., Hirschmann, M.M., Jacobsen, S.D., Le Losq, C., 2019. Raman spectroscopy study of C-O-H-N speciation in reduced basaltic glasses: implications for reduced planetary mantles. Geochim. Cosmochim. Acta 265, 32–47. https://doi.org/10.1016/J.GCA.2019.08.029.
Davidson, J., Wadhwa, M., Hervig, R.L., Stephant, A., 2020. Water on Mars: insights from apatite in regolith breccia Northwest Africa 7034. Earth Planet. Sci. Lett. 552, 116597 https://doi.org/10.1016/J.EPSL.2020.116597.
Etiope, G., Oehler, D.Z., Allen, C.C., 2011. Methane emissions from Earth's degassing: implications for Mars. Planet. Space Sci. 59, 182–195. https://doi.org/10.1016/J.PSS.2010.06.003.
Franz, H.B., Trainer, M.G., Malespin, C.A., Mahaffy, P.R., Atreya, S.K., Becker, R.H., Benna, M., Conrad, P.G., Eigenbrode, J.L., Freissinet, C., Manning, H.L.K., Prats, B.D., Raaen, E., Wong, M.H., 2017. Initial SAM calibration gas experiments on Mars: quadrupole mass spectrometer results and implications. Planet. Space Sci. 138, 44–54. https://doi.org/10.1016/J.PSS.2017.01.014.
Gleason, J.D., Kring, D.A., Hill, D.H., Boynton, W.V., 1997. Petrography and bulk chemistry of Martian orthopyroxenite ALH84001: implications for the origin of secondary carbonates. Geochim. Cosmochim. Acta 61, 3503–3512. https://doi.org/10.1016/S0016-7037(97)00173-7.
Grenfell, J.L., Wunderlich, F., Sinnhuber, M., Herbst, K., Lehmann, R., Scheucher, M., Gebauer, S., Arnold, G., Rauer, H., 2022. Atmospheric processes affecting methane on Mars. Icarus 382, 114940. https://doi.org/10.1016/J.ICARUS.2022.114940.
Gross, J., Filiberto, J., Bell, A.S., 2013. Water in the martian interior: evidence for terrestrial MORB mantle-like volatile contents from hydroxyl-rich apatite in olivine–phyric shergottite NWA 6234. Earth Planet. Sci. Lett. 369–370, 120–128. https://doi.org/10.1016/J.EPSL.2013.03.016.
Heap, M.J., Byrne, P.K., Mikhail, S., 2017. Low surface gravitational acceleration of Mars results in a thick and weak lithosphere: implications for topography, volcanism, and hydrology. Icarus 281, 103–114. https://doi.org/10.1016/J.ICARUS.2016.09.003.
Helgeson, H.C., Kirkham, D.H., 1976. Theoretical prediction of the thermodynamic properties of aqueous electrolytes at high pressures and temperatures. III. Equation

of state for aqueous species at infinite dilution. Am. J. Sci. 276, 97–240. https://doi.org/10.2475/AJS.276.2.97.
Helgeson, H.C., Kirkham, D.H., 1974a. Theoretical prediction of the thermodynamic behavior of aqueous electrolytes at high pressures and temperatures; II, Debye-Huckel parameters for activity coefficients and relative partial molal properties. Am. J. Sci. 274, 1199–1261. https://doi.org/10.2475/AJS.274.10.1199.
Helgeson, H.C., Kirkham, D.H., 1974b. Theoretical prediction of the thermodynamic behavior of aqueous electrolytes at high pressures and temperatures; I, Summary of the thermodynamic/electrostatic properties of the solvent. Am. J. Sci. 274, 1089–1198. https://doi.org/10.2475/AJS.274.10.1089.
Helgeson, H.C., Kirkham, D.H., Flowers, G.C., 1981. Theoretical prediction of the thermodynamic behavior of aqueous electrolytes by high pressures and temperatures; IV, Calculation of activity coefficients, osmotic coefficients, and apparent molal and standard and relative partial molal properties to 600 degrees C and 5kb. Am. J. Sci. 281, 1249–1516. https://doi.org/10.2475/AJS.281.10.1249.
Hirschmann, M.M., Withers, A.C., 2008. Ventilation of $CO_2$ from a reduced mantle and consequences for the early Martian greenhouse. Earth Planet. Sci. Lett. 270, 147–155. https://doi.org/10.1016/J.EPSL.2008.03.034.
Howarth, G.H., Pernet-Fisher, J.F., Balta, J.B., Barry, P.H., Bodnar, R.J., Taylor, L.A., 2014. Two-stage polybaric formation of the new enriched, pyroxene-oikocrystic, lherzolitic shergottite, NWA 7397. Meteorit. Planet. Sci. 49, 1812–1830. https://doi.org/10.1111/MAPS.12357.
Huang, F., Sverjensky, D.A., 2020. Mixing of carbonatitic into saline fluid during panda diamond formation. Geochim. Cosmochim. Acta 284, 1–20. https://doi.org/10.1016/J.GCA.2020.06.011.
Huang, F., Sverjensky, D.A., 2019. Extended Deep Earth Water Model for predicting major element mantle metasomatism. Geochim. Cosmochim. Acta 254, 192–230. https://doi.org/10.1016/j.gca.2019.03.027.
Kite, E.S., Gao, P., Goldblatt, C., Mischna, M.A., Mayer, D.P., Yung, Y.L., 2017. Methane bursts as a trigger for intermittent lake-forming climates on post-Noachian Mars. Nat. Geosci. 10, 737–740. https://doi.org/10.1038/ngeo3033.
Kite, E.S., Mischna, M.A., Gao, P., Yung, Y.L., Turbet, M., 2020. Methane release on Early Mars by atmospheric collapse and atmospheric reinflation. Planet. Space Sci. 181, 104820 https://doi.org/10.1016/J.PSS.2019.104820.
Knapmeyer-Endrun, B., Panning, M.P., Bissig, F., Joshi, R., Khan, A., Kim, D., Lekić, V., Tauzin, B., Tharimena, S., Plasman, M., Compaire, N., Garcia, R.F., Margerin, L., Schimmel, M., Stutzmann, É., Schmerr, N., Bozdag, E., Plesa, A.C., Wieczorek, M.A., Broquet, A., Antonangeli, D., McLennan, S.M., Samuel, H., Michaut, C., Pan, L., Smrekar, S.E., Johnson, C.L., Brinkman, N., Mittelholz, A., Rivoldini, A., Davis, P.M., Lognonné, P., Pinot, B., Scholz, J.R., Stähler, S., Knapmeyer, M., van Driel, M., Giardini, D., Banerdt, W.B., 2021. Thickness and structure of the martian crust from InSight seismic data. Science 373, 438–443. https://doi.org/10.1126/science.abf8966 (1979).
Liu, J., Michalski, J.R., Tan, W., He, H., Ye, B., Xiao, L., 2021. Anoxic chemical weathering under a reducing greenhouse on early Mars. Nat. Astron. 5, 503–509. https://doi.org/10.1038/s41550-021-01303-5.
Manning, C.E., Shock, E.L., Sverjensky, D.A., 2013. The chemistry of carbon in aqueous fluids at crustal and upper-mantle conditions: experimental and theoretical constraints. Rev. Mineral. Geochem. 75, 109–148. https://doi.org/10.2138/rmg.2013.75.5.
McCubbin, F.M., Boyce, J.W., Srinivasan, P., Santos, A.R., Elardo, S.M., Filiberto, J., Steele, A., Shearer, C.K., 2016. Heterogeneous distribution of $H_2O$ in the Martian interior: implications for the abundance of $H_2O$ in depleted and enriched mantle sources. Meteorit. Planet. Sci. 51, 2036–2060. https://doi.org/10.1111/MAPS.12639.
Mikhail, S., Barry, P.H., Sverjensky, D.A., 2017. The relationship between mantle pH and the deep nitrogen cycle. Geochim. Cosmochim. Acta 209, 149–160. https://doi.org/10.1016/J.GCA.2017.04.007.
Mikhail, S., Rinaldi, M., Mare, E.R., Sverjensky, D.A., 2021. A genetic metasomatic link between eclogitic and peridotitic diamond inclusions. Geochem. Perspect. Lett. 17, 33–38. https://doi.org/10.7185/GEOCHEMLET.2111.
Mikhail, S., Sverjensky, D.A., 2014. Nitrogen speciation in upper mantle fluids and the origin of Earth's nitrogen-rich atmosphere. Nat. Geosci. 7, 816–819. https://doi.org/10.1038/ngeo2271.
Miron, G.D., Leal, A.M.M., Yapparova, A., 2019. Thermodynamic properties of aqueous species calculated using the HKF model: how do different thermodynamic and electrostatic models for solvent water affect calculated aqueous properties? Geofluids 2019. https://doi.org/10.1155/2019/5750390.
Montesi, L.G.J., Zuber, M.T., 2003. Clues to the lithospheric structure of Mars from wrinkle ridge sets and localization instability. J. Geophys. Res. 108, 5048. https://doi.org/10.1029/2002JE001974.
Mysen, B., 2014. Water-melt interaction in hydrous magmatic systems at high temperature and pressure. Prog. Earth Planet. Sci. 1, 1–18. https://doi.org/10.1186/2197-4284-1-4/FIGURES/23.
Nicklas, R.W., Day, J.M.D., Vaci, Z., Udry, A., Liu, Y., Tait, K.T., 2021. Uniform oxygen fugacity of shergottite mantle sources and an oxidized martian lithosphere. Earth Planet. Sci. Lett. 564, 116876 https://doi.org/10.1016/J.EPSL.2021.116876.
Peña-Alvarez, M., Brovarone, A.V., Donnelly, M.E., Wang, M., Dalladay-Simpson, P., Howie, R., Gregoryanz, E., 2021. *In-situ* abiogenic methane synthesis from diamond and graphite under geologically relevant conditions. Nat. Commun. 12, 1–5. https://doi.org/10.1038/S41467-021-26664-3.
Piercy, J.D., Bridges, J.C., Hicks, L.J., 2022. Carbonate dissolution and replacement by odinite and saponite in the Lafayette nakhlite: part of the $CO_2$-$CH_4$ cycle on Mars? Geochim. Cosmochim. Acta 326, 97–118. https://doi.org/10.1016/J.GCA.2022.02.003.
Rahib, R.R., Udry, A., Howarth, G.H., Gross, J., Paquet, M., Combs, L.M., Laczniak, D.L., Day, J.M.D., 2019. Mantle source to near-surface emplacement of enriched and intermediate poikilitic shergottites in Mars. Geochim. Cosmochim. Acta 266, 463–496. https://doi.org/10.1016/j.gca.2019.07.034.
Ramirez, R.M., Kopparapu, R., Zugger, M.E., Robinson, T.D., Freedman, R., Kasting, J.F., 2013. Warming early Mars with $CO_2$ and $H_2$. Nat. Geosci. 7, 59–63. https://doi.org/10.1038/ngeo2000.
Rinaldi, M., Mikhail, S., Sverjensky, D.A., Kalita, J., 2023. The importance of carbon to the formation and composition of silicates during mantle metasomatism. Geochim. Cosmochim. Acta. https://doi.org/10.1016/j.gca.2023.06.025 in press.
Samuel, H., Lognonné, P., Panning, M., Lainey, V., 2019. The rheology and thermal history of Mars revealed by the orbital evolution of Phobos. Nature 569, 523–527. https://doi.org/10.1038/s41586-019-1202-7.
Shock, E.L., 1988. Organic acid metastability in sedimentary basins. Geology 16, 886–890. https://doi.org/10.1130/0091-7613(1988)016<0886:OAMISB>2.3.CO;2.
Shock, E.L., Helgeson, H.C., 1988. Calculation of the thermodynamic and transport properties of aqueous species at high pressures and temperatures: correlation algorithms for ionic species and equation of state predictions to 5kb and 1000°C. Geochim. Cosmochim. Acta 52, 2009–2036. https://doi.org/10.1016/0016-7037(88)90181-0.
Shock, E.L., Sassani, D.C., Willis, M., Sverjensky, D.A., 1997. Inorganic species in geologic fluids: correlations among standard molal thermodynamic properties of aqueous ions and hydroxide complexes. Geochim. Cosmochim. Acta 61, 907–950. https://doi.org/10.1016/S0016-7037(96)00339-0.
Steele, A., McCubbin, F.M., Fries, M., Kater, L., Boctor, N.Z., Fogel, M.L., Conrad, P.G., Glamoclija, M., Spencer, M., Morrow, A.L., Hammond, M.R., Zare, R.N., Vicenzi, E. P., Siljeström, S., Bowden, R., Herd, C.D.K., Mysen, B.O., Shirey, S.B., Amundsen, H. E.F., Treiman, A.H., Bullock, E.S., Jull, A.J.T., 2012. A reduced organic carbon component in martian basalts. Science 337, 212–215. https://doi.org/10.1126/science.1220715 (1979).
Sverjensky, D., Daniel, I., Vitale Brovarone, A., 2020. The changing character of carbon in fluids with pressure: Organic geochemistry of Earth's upper mantle fluids. In: Manning, C.E., Lin, J.F., Mao, W.L. (Eds.), Carbon in Earth's Interior. Geophysical Monograph Series, 249, pp. 259–269. https://doi.org/10.1002/9781119508229.CH22.
Stevenson, D.J., 2003. Styles of mantle convection and their influence on planetary evolution. C. R. Geosci. 335, 99–111. https://doi.org/10.1016/S1631-0713(03)00009-9.
Sverjensky, D.A., 2019. Thermodynamic modelling of fluids from surficial to mantle conditions. J. Geol. Soc. Lond. 176, 348–374. https://doi.org/10.1144/jgs2018-105.
Sverjensky, D.A., Harrison, B., Azzolini, D., 2014a. Water in the deep Earth: the dielectric constant and the solubilities of quartz and corundum to 60kb and 1200°C. Geochim. Cosmochim. Acta 129, 125–145. https://doi.org/10.1016/J.GCA.2013.12.019.
Sverjensky, D.A., Huang, F., 2015. Diamond formation due to a pH drop during fluid-rock interactions. Nat. Commun. 6, 8702. https://doi.org/10.1038/ncomms9702.
Sverjensky, D.A., Shock, E.L., Helgeson, H.C., 1997. Prediction of the thermodynamic properties of aqueous metal complexes to 1000°C and 5kb. Geochim. Cosmochim. Acta 61, 1359–1412. https://doi.org/10.1016/S0016-7037(97)00009-4.
Sverjensky, D.A., Stagno, V., Huang, F., 2014b. Important role for organic carbon in subduction-zone fluids in the deep carbon cycle. Nat. Geosci. 7, 909–913. https://doi.org/10.1038/ngeo2291.
Taysum, B.M., Palmer, P.I., 2020. Photochemistry of methane and ethane in the Martian atmosphere. J. Geophys. Res. Planets 125, e2020JE006491. https://doi.org/10.1029/2020JE006491.
Treiman, A.H., 2005. The nakhlite meteorites: augite-rich igneous rocks from Mars. Geochemistry 65, 203–270. https://doi.org/10.1016/J.CHEMER.2005.01.004.
Tsuno, K., Grewal, D.S., Dasgupta, R., 2018. Core-mantle fractionation of carbon in Earth and Mars: the effects of sulfur. Geochim. Cosmochim. Acta 238, 477–495. https://doi.org/10.1016/J.GCA.2018.07.010.
Udry, A., Howarth, G.H., Lapen, T.J., Righter, M., 2017. Petrogenesis of the NWA 7320 enriched martian gabbroic shergottite: insight into the martian crust. Geochim. Cosmochim. Acta 204, 1–18. https://doi.org/10.1016/J.GCA.2017.01.032.
Wang, C., Tao, R., Walters, J.B., Höfer, H.E., Zhang, L., 2022. Favorable P–T–fO2 conditions for abiotic $CH_4$ production in subducted oceanic crusts: a comparison between $CH_4$-bearing ultrahigh- and $CO_2$-bearing high-pressure eclogite. Geochim. Cosmochim. Acta 336, 269–290. https://doi.org/10.1016/J.GCA.2022.09.010.
Webster, C.R., Mahaffy, P.R., Atreya, S.K., Flesch, G.J., Farley, K.A., MSL Science Team, 2013. Low upper limit to methane abundance on Mars. Science 342, 355–357. https://doi.org/10.1126/science.1242902 (1979).
Wetzel, D.T., Rutherford, M.J., Jacobsen, S.D., Hauri, E.H., Saal, A.E., 2013. Degassing of reduced carbon from planetary basalts. Proc. Natl. Acad. Sci. U. S. A. 110, 8010–8013. https://doi.org/10.1073/pnas.1219266110.
Wolery, T.J., 1992. EQ3NR, a computer program for geochemical aqueous speciation-solubility calculations: theoretical manual, user's guide, and related documentation (version 7.0). Lawrence Livermore National Laboratory, University of California, Livermore, CA.
Wordsworth, R., Kalugina, Y., Lokshtanov, S., Vigasin, A., Ehlmann, B., Head, J., Sanders, C., Wang, H., 2017. Transient reducing greenhouse warming on early Mars. Geophys. Res. Lett. 44, 665–671. https://doi.org/10.1002/2016GL071766.
Ye, B., Michalski, J.R., 2022. Chemical weathering over hundreds of millions of years of greenhouse conditions on Mars. Commun. Earth. Environ. 3, 1–14. https://doi.org/10.1038/s43247-022-00602-7.
Yung, Y.L., Chen, P., Nealson, K., Atreya, S., Beckett, P., Blank, J.G., Ehlmann, B., Eiler, J., Etiope, G., Ferry, J.G., Forget, F., Gao, P., Hu, R., Kleinböhl, A., Klusman, R., Lefèvre, F., Miller, C., Mischna, M., Mumma, M., Newman, S., Oehler, D., Okumura, M., Oremland, R., Orphan, V., Popa, R., Russell, M., Shen, L., Sherwood

Lollar, B., Staehle, R., Stamenković, V., Stolper, D., Templeton, A., Vandaele, A.C., Viscardy, S., Webster, C.R., Wennberg, P.O., Wong, M.L., Worden, J., 2018. Methane on Mars and habitability: challenges and responses. Astrobiology 18, 1221. https://doi.org/10.1089/AST.2018.1917.

Zhang, C., Duan, Z., 2009. A model for C-O-H fluid in the Earth's mantle. Geochim. Cosmochim. Acta 73, 2089–2102. https://doi.org/10.1016/j.gca.2009.01.021.

Zhang, L., Zhang, L., Tang, M., Wang, X., Tao, R., Xu, C., Bader, T., 2023. Massive abiotic methane production in eclogite during cold subduction. Natl. Sci. Rev. 10 https://doi.org/10.1093/NSR/NWAC207.

Zhang, X., Berkinsky, D., Markus, C.R., Chitturi, S.R., Grieman, F., Okumura, M., Luo, Y., Yung, Y.L., Sander, S.P., 2021. Reaction of methane and UV-activated perchlorate: relevance to heterogeneous loss of methane in the atmosphere of mars. Icarus 376, 114832. https://doi.org/10.1016/j.icarus.2021.114832.

Zolotov, M., Shock, E., 1999. Abiotic synthesis of polycyclic aromatic hydrocarbons on Mars. J. Geophys. Res. Planets 104, 14033–14049. https://doi.org/10.1029/1998JE000627.

Zolotov, M.Y., Shock, E.L., 2000. A thermodynamic assessment of the potential synthesis of condensed hydrocarbons during cooling and dilution of volcanic gases. J. Geophys. Res. Solid Earth 105, 539–559. https://doi.org/10.1029/1999JB900369.